Interconnection and lamination technologies towards ubiquitous integration of photovoltaics

Peer-reviewed author version

GOVAERTS, Jonathan; BORGERS, Tom; LUO, Bin; VAN DYCK, Rik; VAN DER HEIDE, Arvid; REEKMANS, Bart; VASTMANS, Luc; Moors , Reinoud; Doumen, Geert; TOUS, Loic & POORTMANS, Jef (2023) Interconnection and lamination technologies towards ubiquitous integration of photovoltaics. In: PROGRESS IN PHOTOVOLTAICS, 31 (11), p. 1114-1129.

DOI: 10.1002/pip.3730
Handle: http://hdl.handle.net/1942/40767

Interconnection and Lamination Technologies towards Ubiquitous PV Integration

Jonathan Govaerts[1,2,3], Tom Borgers[1,2,3], Bin Luo[1,2,3,4], Rik Van Dyck[1,2,3,4], Arvid van der Heide[1,2,3], Bart Reekmans[1,2,3], Luc Vastmans[1,2,3], Reinoud Moors[1,2,3], Geert Doumen[1,2,3], Loic Tous[1,2,3] and Jef Poortmans[1,2,3,4]
[1]imec, imo-imomec, Genk, Belgium
[2]EnergyVille, imo-imomec, Genk, Belgium
[3]Hasselt University, imo-imomec, Hasselt, Belgium
[4]KULeuven, Leuven, Belgium

Abstract:

In this paper we first give some historical background and trends in PV module technologies with a focus on the growing trend towards "PV everywhere", mainly targeting improved aesthetics, dimensional freedom including curved surfaces, weight concerns and specific reliability testing. This section acts as an introductory review of the field.

Then, in the following sections, we elaborate on two technological developments in this field where we are active: (i) multi-wire interconnection and (ii) advanced encapsulation.

In terms of multi-wire interconnection, this technology offers improved aesthetics, a similar performance and dimensional freedom compared to the traditional tabbing-stringing process, and the experiments show promising results on extended reliability testing, including thermal cycling, damp heat and humidity freeze, as well as high-temperature storage.

In terms of advanced encapsulation, we introduce our approach for curved surfaces using a double-membrane laminator and present results on fabricating curved modules, targeting as demonstration examples on the one hand, glass-glass sunroofs, and on the other hand, lighter-weight bonnets for automotive applications.

We mix examples targeting building and automotive applications, to illustrate the variety of requirements (colours, curvature, weight, reliability, safety), although this variety within building and vehicle applications is probably as large as between them.

Keywords: Integrated PV, aesthetics, curved PV, light-weight materials, reliability testing

1. INTRODUCTION: BACKGROUND REVIEW

Historically, PV modules have mostly been implemented in a way to maximize energy generation, reduce the PV levelized cost of electricity, and (deliberately or not) promote the PV asset user/owner as being environmentally conscious. In many cases, this often leads to PV modules being very visible, with the typical pattern of blue (semi-)squares of the solar cells on a white module background. Gradually however, PV installations have grown to be more mainstream and are slowly becoming ubiquitous in urban environments. In particular that is the case in the developed world and the built environment where PV is either legally required or profitable (or both) in new projects, while also the necessary prefinancing is typically available. In a similar way, also all kinds of vehicles and the transportation sector in general are slowly becoming a market of interest for PV (integration) [1].

All this means that PV is ever more present in our daily lives and its typical appearance is experienced as uncomfortably unattractive by some to even downright unacceptable by others. Because of this, in recent years, there is a growing trend towards a more unobtrusive appearance. As a low-hanging fruit that was picked up very early on, a black backsheet was implemented to replace the white background, immediately subduing the "blue squares" pattern that is visible from afar. In the same makeover, also the bare Al frame was replaced with a black (anodized)

Al version. This could already resolve most of the concerns of building owners related to the aesthetics of their roofs and facades that are far enough away. After this, and coming closer to the PV module, the interconnect wiring is the next eyecatcher coming into view. To address this effect, a recent trend that is gaining traction in industry is to distribute the cell interconnect wiring more evenly across the cell surface (adding more ribbons but with smaller cross-section) to create a more uniform appearance on the cell area (with additional benefits in terms of resistive and/or optical gains in a trade-off with the cell metallization cost). The next step, or alternative step, is to hide the visible metallic wiring in and outside of the active area. This can be done by painting the ribbons (before or after stringing) or by adding a black material in front within the lamination stack. Both approaches imply an increased process complexity and cost, for only a limited aesthetical gain, compared to the previous adaptations, that either were simply a replacement (backsheet or frame), or were combined with an improved performance/cost (wiring redistribution). The above evolutions are illustrated in Figure 1.

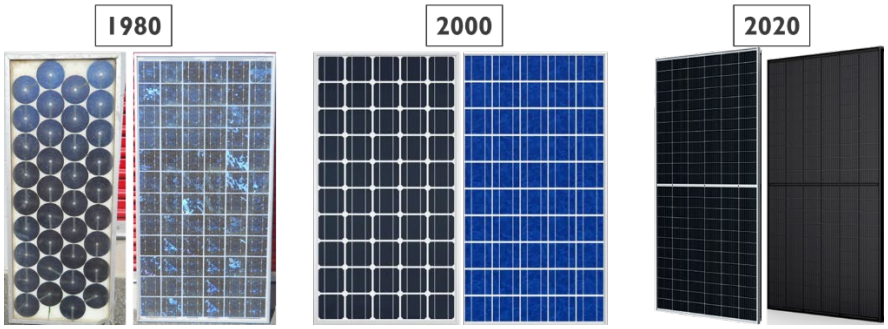

Figure 1: Historical evolution of (aesthetics of) c-Si PV modules: initial small c-Si modules with round monocrystalline or square multicrystalline Si solar cells (left, 1980 [2]), evolving into larger modules with semisquare monocrystalline or square multicrystalline Si solar cells (middle, 2000 [3]) and high-volume produced modules with half-cut (mostly monocrystalline) Si solar cells with multi-busbar interconnection and either white or black backsheet and frame (right, 2020 [4])

More recently, shingling technology [5] is gaining more and more attention in this field. In this approach, the cells are cut in stripes and interconnection is done by overlapping the cells. This way, the busbars for collecting the current from the finger metallization are hidden behind the neighbouring cell (shingle) that is put in series, and thus, in terms of aesthetics, the appeareance can be more homogeneous. Additionally, since the stripes (shingles) overlap and are much narrower than full cells, it is easier to maximize the active (Si) area on a complex surface for integrated applications.

Outside the scope here, but for completeness: in parallel, back-contact modules based on Metal Wrap Through (MWT) or Interdigitated Back Contacted (IBC) cells offer the inherent benefits of improved aesthetics and performance, due to the minimization of metallization on the frontside of the cell, albeit at the cost of additional process complexity and associated costs [6].

In a later evolution that is currently picking up speed, the challenge is to hide the modules in plain sight, even at the cost of a (significantly) reduced performance and increased material costs. The underlying idea is that additional surfaces may thus be unlocked for PV electricity generation. Options in various stages of development include colouring of glass [7], foils [8,9] or textiles [10] in front of the cells, up to assembling even semi-transparent stone or wood veneer in front [11]. A more detailed review has been published by PVPS task 15 [12]. These and more concepts are illustrated in Figure 2.

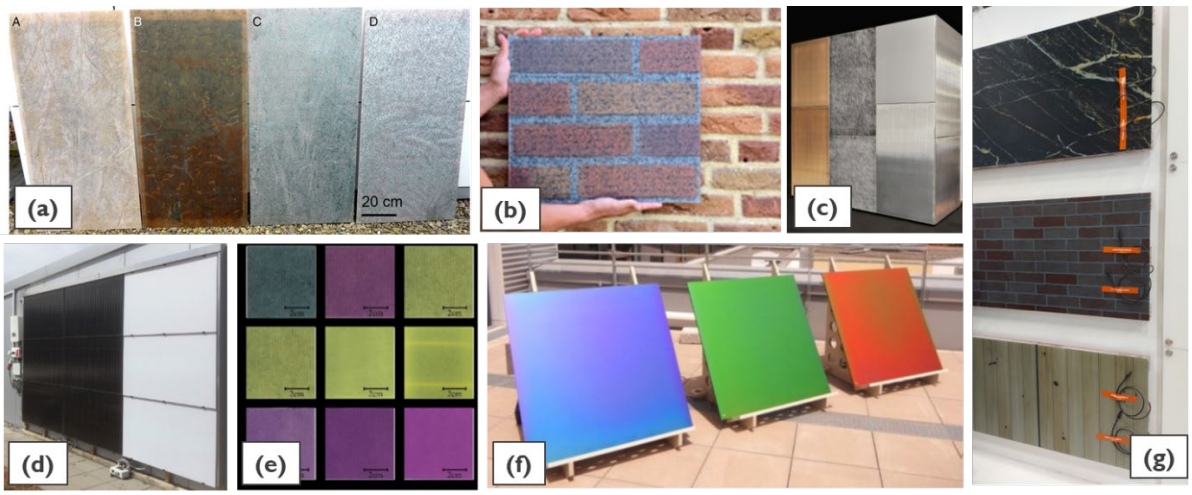

Figure 2: PV encapsulation approaches sacrificing some performance for improved aesthetics: (a) stone veneer as front surface of the PV laminate [11]; (b) colour pattern implemented on a film in the laminate, with design taking into account the underlying cell appearance [9]; (c,d) white/coloured film implemented in the laminate [8]; (e) coloured textile implemented in front of the front glass [10]; (f) Bragg reflector implemented on the (inner) glass surface [13]; (g) colour pattern printed on and fused to the front glass, honeycomb lightweight support at the rear [14]

Beyond the hiding of the PV cells behind or blending them uniformly in the module's colours, the next level of PV integration entails enabling advanced form factors such as curved surfaces for an even wider range of applications, both architectural and automotive (e.g. in passenger vehicles). For this, the cells as well as the interconnection should of course withstand the imposed curvatures and stresses, but the most challenging is probably the encapsulation process. The current standard technology for PV encapsulation is based on single membrane flat-plate lamination [15]. However, as such, it does not allow to laminate curved surfaces. To this end, a range of approaches are being implemented. Staying close to standard lamination, one option is to keep the same (flat) process and bend the module after lamination, either while it is still hot, or after cool-down. Depending on the bill-of-materials (type and thickness), the module will need additional fixation (gluing, frame clamping, ...) to keep its (curved) form [16]. A second option is to adapt the lamination equipment. A typical adaptation in this approach is to include an additional mould support during the lamination [17]. The drawback here is the complexity related to its influence on the thermal behaviour (speed and uniformity of heating and cooling). From another perspective, with more affinity to the glass industry, people are looking into vacuum bagging and autoclaving approaches [17]. A hybrid approach is based on a membrane laminator that is equipped with an additional bottom membrane. These concepts are illustrated in Figure 3. Additional approaches are conceivable, including a somewhat obvious modification of a flat plate laminator (e.g. [18]) for curved shapes by substituting the flat plates with moulds.

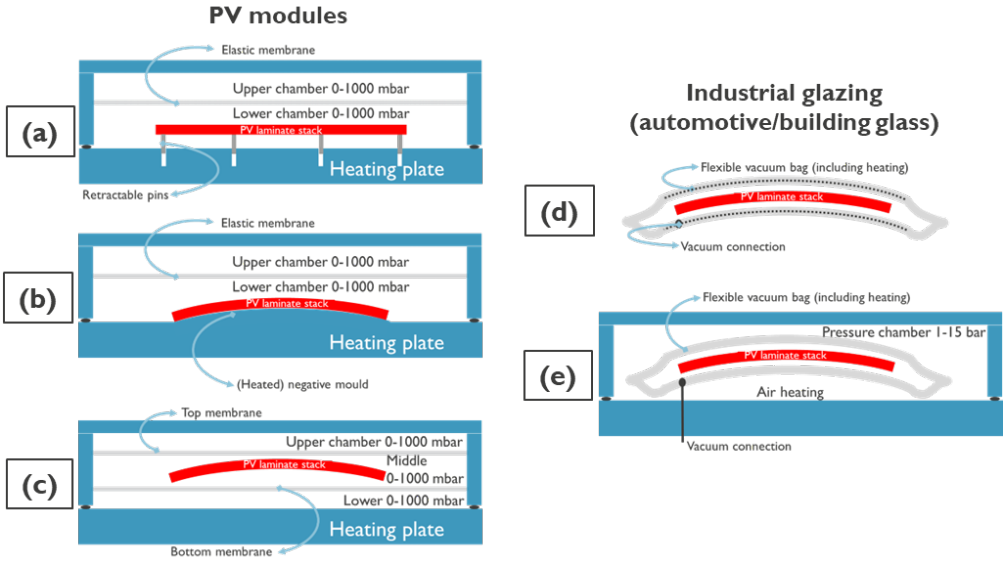

Figure 3: lamination approaches for curved shapes: (a) typical PV single membrane lamination (cold bending afterwards for curved shapes) (b) single membrane lamination with (bottom) negative mould (c) double membrane lamination (d) self-heating vacuum bag (e) vacuum bag in autoclave

Depending on the application, also weight limitations should be considered for the further integration of PV. Again, this can be a prerequisite for buildings, e.g. commercial roofs with limited load-bearing capacity, but even more importantly for the transportation sector, where extra weight in a vehicle is immediately translated into additional energy consumption and reduced autonomy. Dominating the weight of standard PV modules, glass is the first component to scrutinize, given its high density (2500 kg/m^3 or 2.5 kg/m^2 per mm of thickness). Thinner glass can be used, although this will also impact the mechanical stability and fragility. To completely avoid the use of glass sheets, possible alternatives include the use of polymer sheets with or without fibre reinforcement (composites) [19], honeycomb structures [19] and metal, all of which are endemic in various applications, including vehicles and buildings.

Additional application-specific requirements may be required for the final integration, ranging from reliability and lifetime to mechanical and electrical safety. This is beyond the scope of this paper. Also beyond the scope of this paper are other encapsulation technologies that are somewhat further away from current PV module manufacturing, such as vacuum infusion and other liquid-based technologies that have more affinity with composite materials processing [20].

In this background of a growing demand for seamless (and invisible) integration of PV everywhere close to the consumer, we discuss in the following sections some technologies that are in development at imec towards this end. First we elaborate on our multi-wire interconnection technology, where we indicate how it compares to traditional (busbar tabbing-stringing) interconnection in terms of aesthetics, performance, dimensional freedom and reliability. Then we switch to double-membrane lamination, and demonstrate how it allows to extend traditional "flatbed" lamination towards complex surfaces in a flexible way. Two examples are elaborated: a glass-glass sunroof and a car bonnet. For the car bonnet, we discuss the implementation of a fibre-reinforced backsheet, using similarly a double-membrane lamination process, to reduce its weight.

2. MULTI-WIRE INTERCONNECTION TECHNOLOGY

2.1 Approach and method

In previous publications [21] we have reported on a multi-wire (MW) approach based

on hybrid stitch-weaving of wires into so-called interconnect foils. In this technology the wires are implemented in an encapsulant-based foil, distributed over the cell area in order to directly contact the finger metallization of the frontside of one cell and the backside of the neighbouring cell. A solder-based interconnect is established during lamination. The foil preparation is illustrated in Figure 4, as well as the layup process.

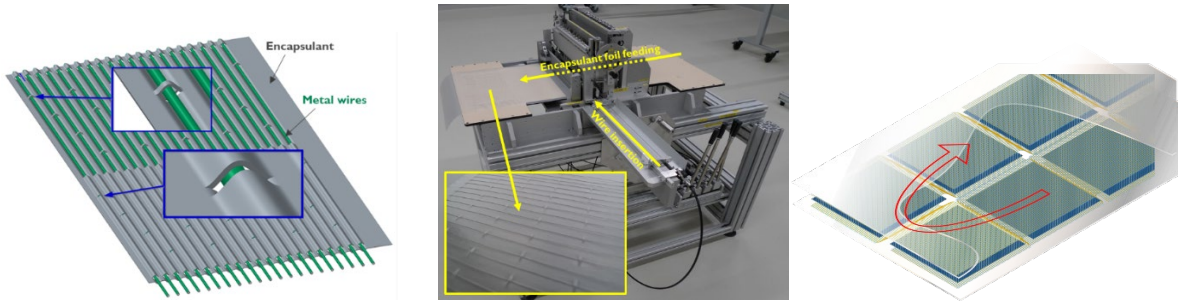

Figure 4: MW interconnection approach: interconnect foil design layout (left), fabrication (middle, with resulting foil zoom in insert) and layup schematic

Alternatingly placing cells and interconnect foils, allows 90 degrees turning at every cell (assuming an appropriate cell metallization). This provides dimensional freedom compared to the 1-dimensional strings from standard tabbing-stringing with bussing ribbons at the end of each string. Thus, different sizes of PV modules may be more efficiently populated with cells, while reducing the amount of bussing and adding flexibility for string length and bypass diode integration. This is illustrated in Figure 5 for a roof slate BIPV product of 0.60 x 1.52 m^2 incorporating 3x9 solar cells. In this example all bussing at the left and right edges is eliminated and the 2 strings can have more similar lengths (13- and 14-cell strings compared to 9- and 18-cell strings).

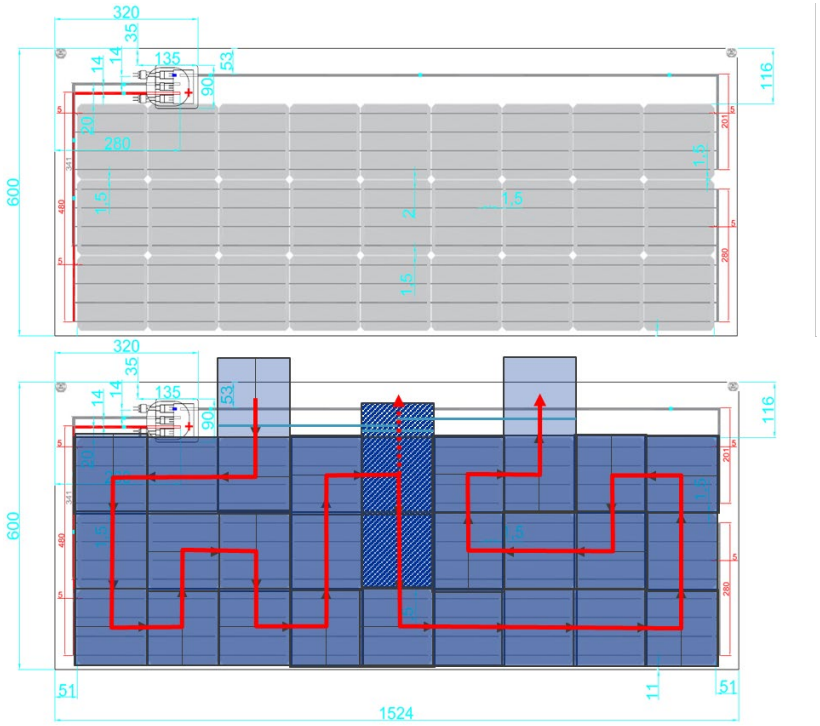

Figure 5: Illustration of dimensional freedom of multi-wire interconnection (bottom) compared to 5BB tabbing-stringing (top) for a BIPV roof slate product

2.2 Aesthetics and performance potential in integrated (BIPV) applications

The MW approach allows for more uniform aesthetics while keeping performance. This is illustrated in Figure 6 and Table 1, for the BIPV roof slate product introduced in Figure 5. The error in measurements is mainly in Isc, 1-2%, due to the uniformity of the used flasher. The only significant difference in performance in Table 1 relates to the V_{oc}, which is highly likely due to the difference in cell performance between similar cells with and without busbars. Though this was not checked in detail (for the lack of measurement capabilities of busbarless cells at that time).

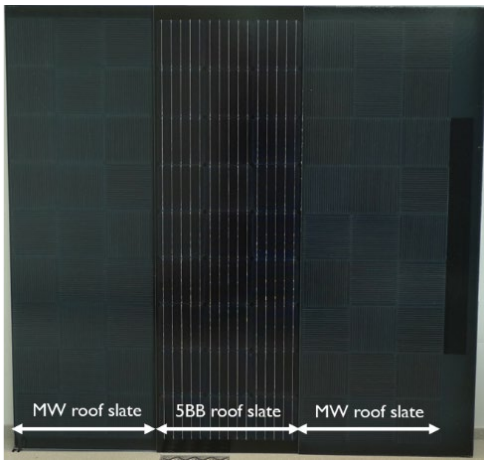

Figure 6: Improvement of multi-wire aesthetics: roof slate product (3x9 cells) comparing 5BB tabbing stringing (centre) with the multi-wire (MW) approach (left and right) for interconnection

Table 1: IV-performance parameters and interconnect cross-section comparing the roof slate PV module with either multi-wire interconnection or 5BB tabbing-stringing (measurement error < 2%)

	I_{sc} [A]	V_{oc} [V]	FF [%]	P_{mpp} [W]	Cross-section [mm^2]
Multi-wire	9.2	18.8	76.8	132	0.9
5BB stringing	9.3	18.4	76.7	132	0.9

To further demonstrate the aesthetics of this multi-wire interconnection technology, we also implemented it in BIPV modules meant for facade integration. In an opaque application, we fabricated and compared glass-glass modules of 1.00 x 0.73 m^2 with a clear front glass ("Blue" in Table 4) and a front glass with a magenta coating on the inner side ("Magenta" in Table 4) [7]. Both types have a black coating on the outer surface of the backside glass. The result is shown in Figure 7 and Table 2.

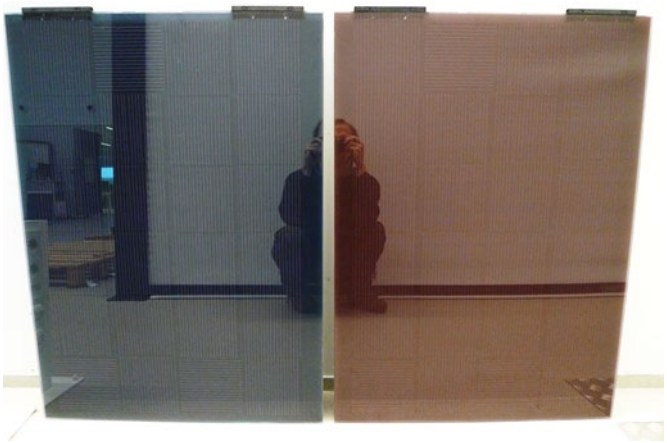

Figure 7: MW interconnection applied for opaque (blue and magenta) BIPV applications: optical impression

Table 2: MW interconnection applied for opaque (blue and magenta) BIPV applications: IV performance (measurement error < 2%)

	I_{sc} [A]	V_{oc} [V]	FF [%]	P_{mpp} [W]
Blue	8.551	17.552	80.5	120.8
Magenta	7.116	17.424	80.9	100.3

Simultaneously, we also compared the multi-wire interconnection for a semi-transparent application against traditional 5BB tabbing-stringing, cf. Figure 8 and Table 3. In this case, the gap between neighbouring cells is increased to 45 mm to allow light to pass through. For this application, the semi-transparent glass-glass modules of 1.00 x 1.00 m^2 are integrated into an insulated glazing unit (IGU) consisting of a spacer and a low-e coated glass.

The differences are mainly in V_{oc} and I_{sc}, and are attributed to the difference in cell performance: the busbarless silicon heterojunction (SHJ) cells used for the MW module have a higher V_{oc} but lower I_{sc} than the PERC cells used for the 5BB module.

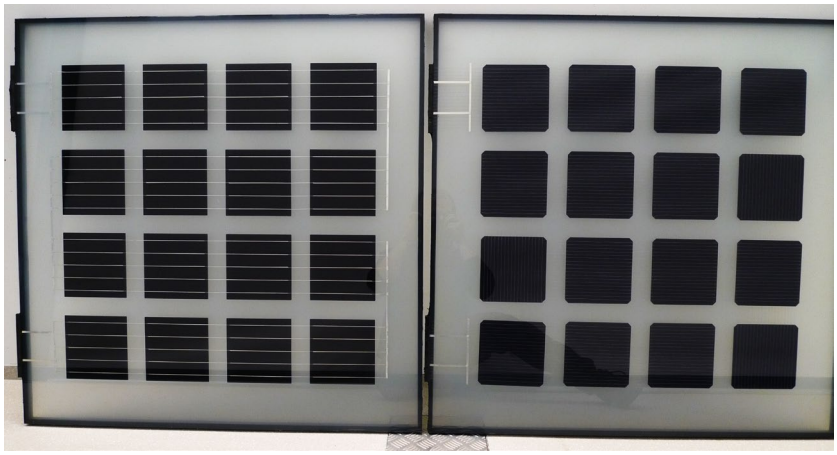

Figure 8: MW interconnection applied for semi-transparent BIPV applications: optical impression of reference 5BB and MW modules integrated into an insulated glazing unit (IGU).

Table 3: MW interconnection applied for semi-transparent BIPV applications: IV performance of reference 5BB and MW modules integrated into an insulated glazing unit (IGU) (measurement error < 2%)

		I_{sc} [A]	V_{oc} [V]	FF [%]	P_{mpp} [W]
5BB		9.460	10.939	76.7	79.4
MW		9.100	11.724	77.1	82.3

2.3 Extended reliability testing

In an updated version of the interconnect foils from [21], by implementing a patented method [22], we have now improved and extended reliability results with regards to thermal cycling (TC; 3h-cycles between 85 and -40°C), damp heat (DH; exposure to 85°C / 85%RH), high-temperature storage (HT; 500h@105°C and 10h@120°C) and humidity freeze cycling (HF; 24-hour cycles between 85°C / 85%RH and -40°C).

We fabricated glass-glass samples with two versions of interconnect foils (MW1 and MW2), either 2x2-cell (TC) or 1-cell (DH, HT and HF) laminates. MW1 is similar to MW2, but

~10%wt of GF was included in the polymer matrix, in an effort to reduce CTE and improve performance in reliability testing [23-24]. In addition, two types of 2x2-cell reference laminates were included each time, using the same polyolefin (PO) encapsulants for both a reference commercial multi-wire approach (MW) using n-type silicon heterojunction (SHJ) cells and a standard 5BB build-up based on PERC-type cells. Table 4 shows the typical starting performance values of the different types and their respective interconnect cross-sections.

Table 4: Representative starting performance of test and reference 2x2-cell samples (measurement error < 2%)

	I_{sc} [A]	V_{oc} [V]	FF [%]	P_{mpp} [W]	Cross-section [mm^2]
MW1	8.49	2.889	76.6	18.784	0.63
MW2	8.55	2.926	78.8	19.701	0.63
MW	8.38	2.921	80.1	19.613	0.88
5BB	8.59	2.626	78.2	17.641	1

Important to note is that MW1 has consistent and reproducible lower starting performance due to shunting that is both visible in the (pseudo-)fill factor (FF) values, Tables 2 and 3, and in the EL pictures (Figures 7 to 11, identical EL exposure parameters of 250 ms at 8A). While the mechanism for this shunting is not yet understood exactly, interestingly, it is related to the cell design/type and it can be recovered with a single exposure to -40°C, as in the TC and HF testing (going in 90 min to -40°C and back, with a dwell time of 10 min at -40°C). This effect is illustrated in Figure 9 and Table 5 for a 1-cell laminate, and could be consistently reproduced, both in single-cell laminates and in 2x2-cell laminates.

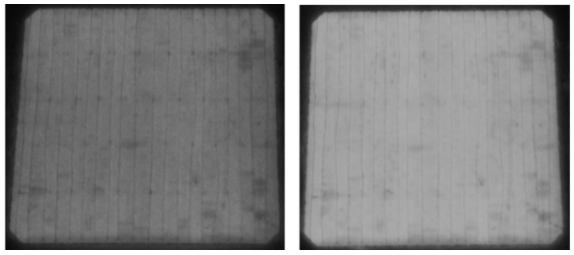

Figure 9: EL pictures (identical exposure parameters of 250 ms at 8A) of an initial shunt (left) in a 1-cell MW1 laminate, that is relieved after exposure to -40°C

Table 5: IV parameters of an initial shunt (left) in a 1-cell MW1 laminate, that is relieved after submission to an exposure to -40°C

	I_{sc} [A]	V_{oc} [V]	FF [%]	P_{mpp} [W]	pFF [%]
After lamination, before exposure to -40ºC	9.053	0.723	74.7	4.889	80.3
After exposure to -40ºC	9.051	0.733	77.7	5.155	83.7

Figures 10 to 13 indicate the degradation of the different sample types for each test, both in terms of Pmpp throughout the test and electroluminescence (EL) comparison between start and end of the test. At first glance, most samples hold up relatively well.

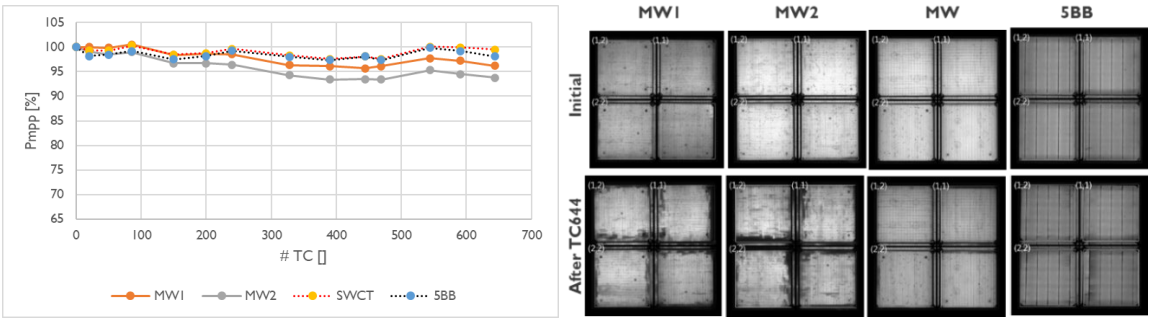

Figure 10: P_{mpp} evolution (left) throughout TC exposure and EL images before and after 644 thermal cycles (right)

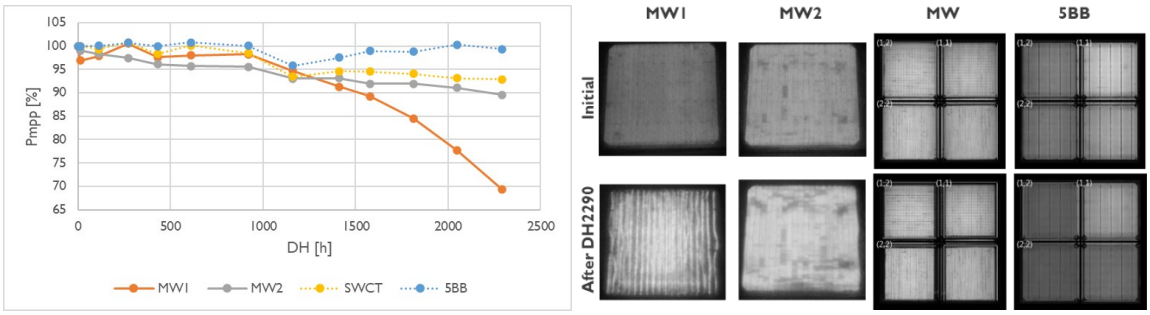

Figure 11: P_{mpp} evolution (left) throughout DH exposure and EL images before and after 2290 h of DH (right)

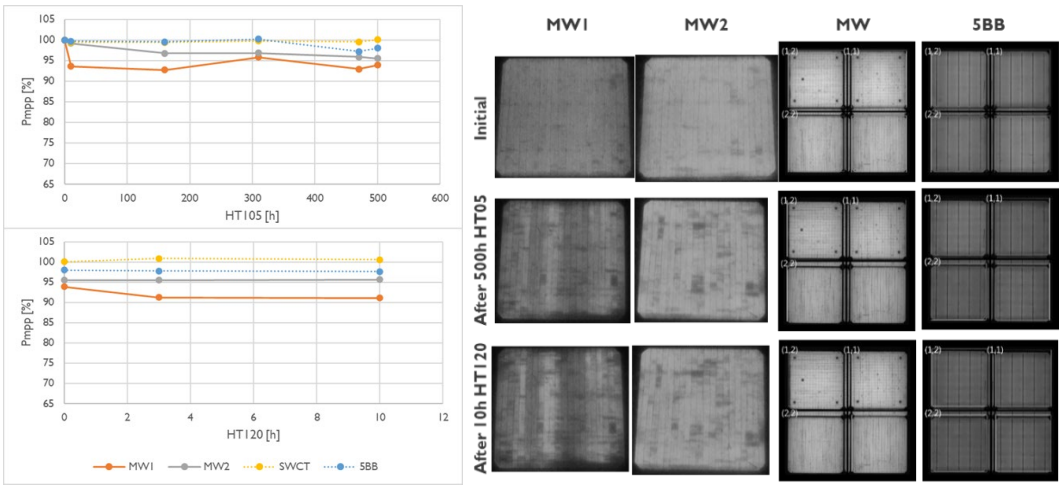

Figure 12: P_{mpp} evolution (left) throughout HT exposure and EL images before and after 500 h of HT105 and after an additional 10 h of HT120 (right)

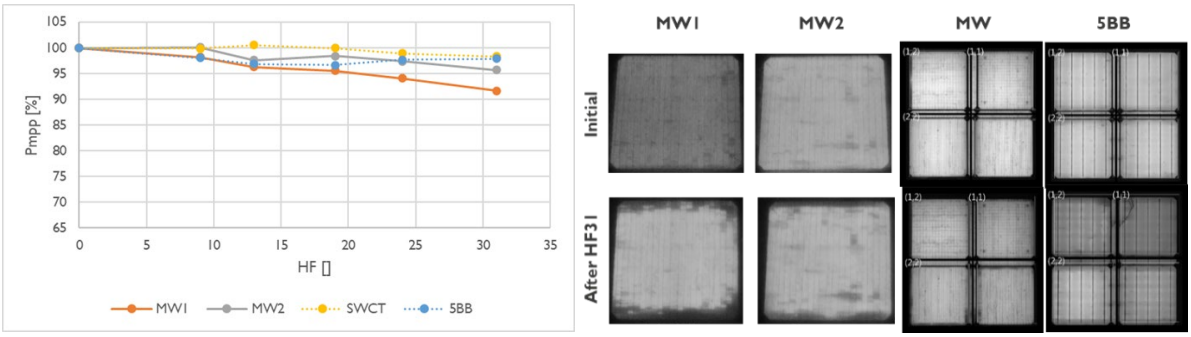

Figure 13: P_{mpp} evolution (left) throughout HF exposure and EL images before and after 31 HF cycles (right)

Overall, based on these results, a few observations can be made. Firstly, all reference samples remain stable throughout the tests. Secondly, MW1 and MW2 exhibit similar degradation, except in DH (see Figure 11), where MW2 outperforms MW1. The degradation pattern in MW1 observed in EL is difficult to interpret though. Zooming in on this a bit further, Figure 14 indicates that the mechanism is probably related to cell degradation, as the wire contacting regions (brighter) are less affected than the regions in between (darker). Comparing the EL picture to the front- and backside wire positions, it seems the (cell) degradation is dominant at the backside. Our hypothesis is that either the p-type a-Si, or the ITO or the Ag finger metallization on that side is affected by the moisture ingress.

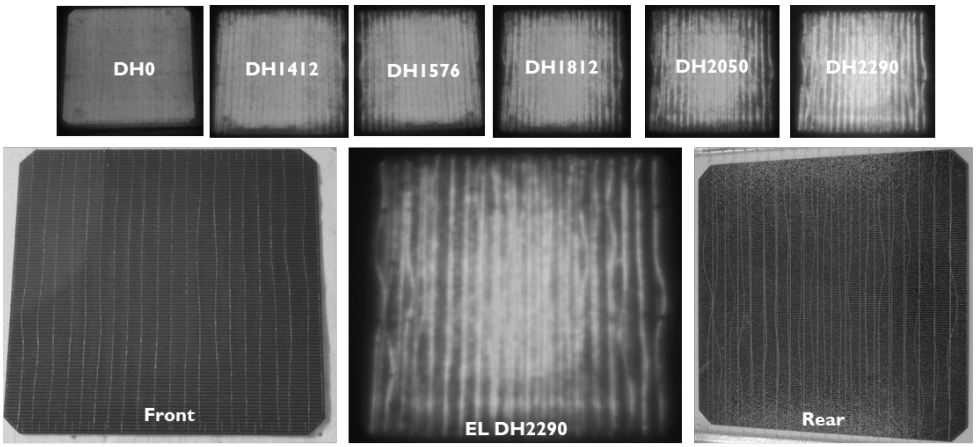

Figure 14: EL degradation pattern throughout DH testing for the MW1 sample (top), and expanded view of the last EL picture (bottom centre) to compare patterns with front- (left) and rearside (right) wires

The fluctuations of MW1 in HT conditions, Figure 12, are attributed to variability in pFF combined with a bad contact of some wires to the bussing ribbons, visible in the EL pictures as the darker vertical regions. Overall, while basic IEC61215 tests in terms of TC, DH and HF can be passed (less than 5% degradation after resp. 200 cycles, 1000h and 10 cycles), some improvement is preferable.

In additional tests with 1-cell laminates, we have also included alternative cell types, encapsulant types and lamination parameters, as a first step towards screening of the process/material "window" of the concept. While a consistent assessment with statistical sample numbers on a comprehensive set of variations is still needed (and planned), the results here, illustrated in the graph in Figure 15 indicate a similar potential:

- Similar degradation for different cells (TOPCon vs SHJ)
- Similar TC degradation with other encapsulants (PO1 vs PO2, EVA and PVB)
- Similar TC degradation with other (set) lamination temperatures (150 vs 165 °C)

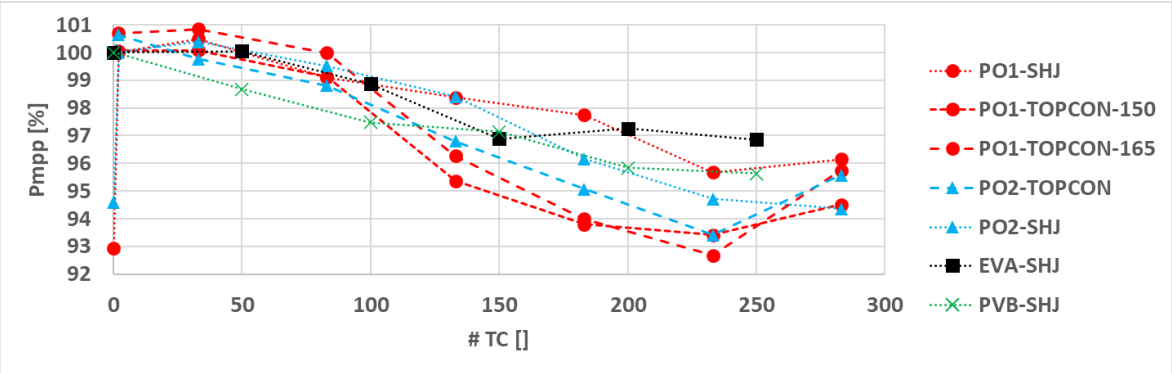

Figure 15: P_{mpp} degradation throughout TC for additional 1-cell laminates, for different cell

types, lamination temperatures, and encapsulants

Interestingly, the initial shunt that was observed earlier for the MW1 samples did reoccur for the SHJ cells that were also used in the first batch, though it is not there for the identical laminates with TOPCon cells, as can also be seen in Figure 15.

It is clear that while the interconnection technology can pass some basic individual tests in the conventional IEC61215 testing for PV modules as well as high-temperature storage testing applied in building and automotive standards, improvements and additional evaluations are still required for commercial deployment. This includes (but is not limited to) hail impact, mechanical load, vibrations and ball impact as well as other variations of climatic tests specified for different applications (IEC1215, IEC TS 62782, ECE R43, ISO 16750-3, ISO 16750-4). The expectation is that such a thing can be (at least partly) addressed by a scale-up towards pilot-line fabrication, by automating, optimizing and tuning the manufacturing processes, both in terms of mechanical fabrication of foils as well as in consistent and reproducible layup actions and lamination materials and processes.

3. DOUBLE-MEMBRANE LAMINATION

3.1 Approach and method

To address curvature requirements, we are looking into a hybrid approach, based on a standard laminator that is equipped with an additional bottom membrane. Figures 16 and 17 illustrate how simultaneously building up the pressure from both the top and bottom membrane allows to laminate complex curvatures without the need for a supporting mould. In fact, such a process is a step in the direction of autoclaving. While the pressure does not rise to the same levels (in the order of 10 bar) though, the heat transfer to the module stack is also reduced because of the air all around (as opposed to the direct contact between glass and hotplate in a standard single-membrane flat-plate lamination). The absence of a mould allows for more flexibility and tolerance in form factor. In the following subsections, we apply this type of lamination for two types of VIPV applications: a glass-glass sunroof (with MW interconnection) and a car bonnet (with shingled interconnection).

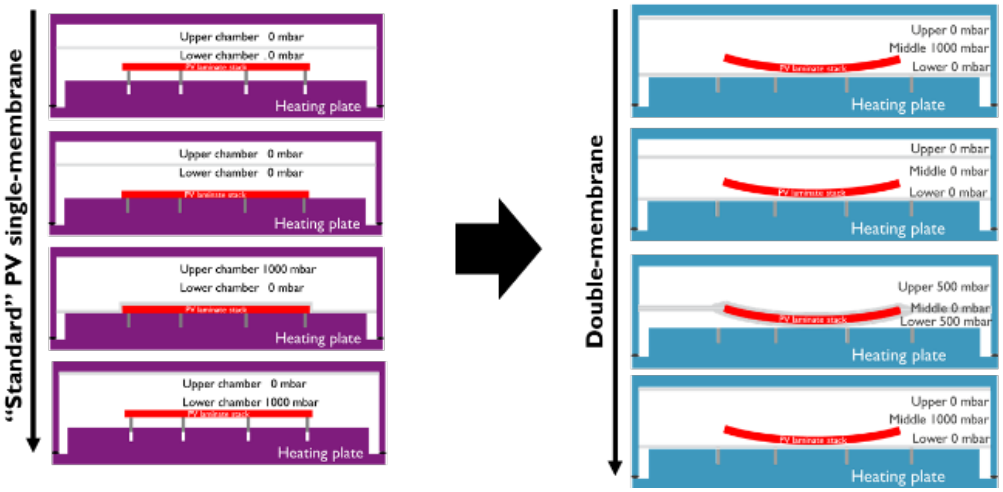

Figure 16: schematic comparison between a typical PV lamination process (top to bottom) with single-membrane (left) and the adaptation in this work to double-membrane lamination (right) for allowing curved surfaces

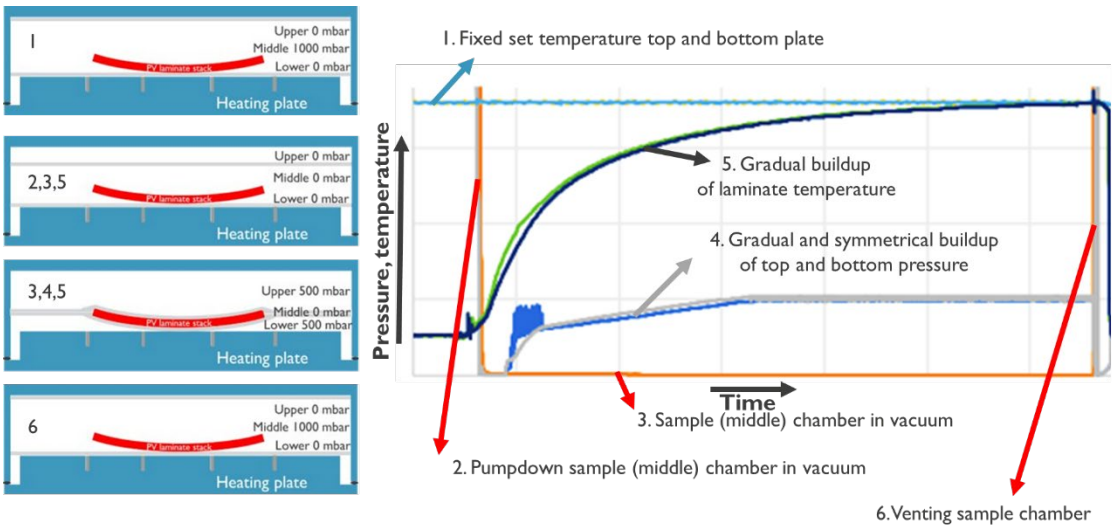

Figure 17: Double-membrane lamination process schematic (left) with associated a graph (right), indicating the symmetrical buildup of top and bottom pressure in the chamber (blue and gray graphs), the inside the chamber (black graph) and the pumpdown and venting of the sample (middle) chamber (orange graph)

Important to note is that an optimization of the recipe is required for each type of integrated PV laminate due to the (possibly) highly different nature of the targeted structure and interconnection technology.

As an illustration, for the glass-glass sunroof in Section 3.2 we used higher-than-typical temperatures (>160degC) and extended times (order of 60 minutes), to reach a sufficiently high temperature inside the laminate for the MW soldering (during lamination). Depending on the glass thickness, it might be useful to even further extend the lamination time. On the other hand, e.g. with the shingled interconnection and the lower thermal mass of the light-weight buildup in the car bonnet in Section 3.3, less high temperatures are required. Also the curvature plays a role in the thermal behaviour (uniformity) and therefore the optimization of the lamination recipe. Similarly, also the pressure can be optimized depending on the laminate buildup. E.g. for the car bonnet we used a very low symmetrical pressure of 50 mbar on both sides, while for the glass-glass sunroof we used symmetrically 500 mbar. The lower pressure might reduce slightly the transfer of heat to the laminate, but in the case of the car bonnet it was necessary to avoid crushing the hollow structure formed by the bonnet top surface and its support.

3.2 (VIPV) application 1: glass-glass sunroof

In a first application, the goal is to integrate PV in the existing sunroof of a car. This involves a glass-glass buildup with a multi-directional curvature, with a minimum curvature radius of 3.5 m, and a maximum height difference of the stack (important to be able to fit in the laminator chamber) of 7 cm between corners and center point of the stack. In first instance, we implement 6 standard strings of 11 half cells (PERC-type) on a glass area of roughly 1.15 x 1.15 m^2. Some issues with frame height, and temperature and pressure (distribution) were addressed by modifying the laminator chamber, the process and the module buildup. Regarding the laminator chamber, the frame height was increased by replacing the spacer frame, increasing the space between the top- and bottom planes of the laminator chamber. Additionally, the lamination pressure was adapted, and steel wool material was added for pressure redistribution. In terms of module buildup, we also adapted the encapsulant type and thickness.

Figure 18 illustrates how non-optimized recipes and laminator preparation can cause glass breakage, but without inducing cracks on the incorporated solar cells. Apart from the frame

chamber height and pressure distribution that may mechanically cause cracks, also thermal stress may induce cracks, due to a non-uniform temperature distribution across the (non-tempered) glass that is used. From this perspective, it is important to limit the temperature non-uniformity during lamination, including, and in particular during the temperature buildup phase. Of course, also the pressure buildup has to be done simultaneously from both sides in the double-membrane configuration. After solving this issue, Table 6 reports on the performance parameters of such PV sunroofs. The improvement in short circuit current (I_{sc}) for the 2nd trial is due to the front glass having a higher transparency. This was confirmed in spectral transmission measurements (not reported here).

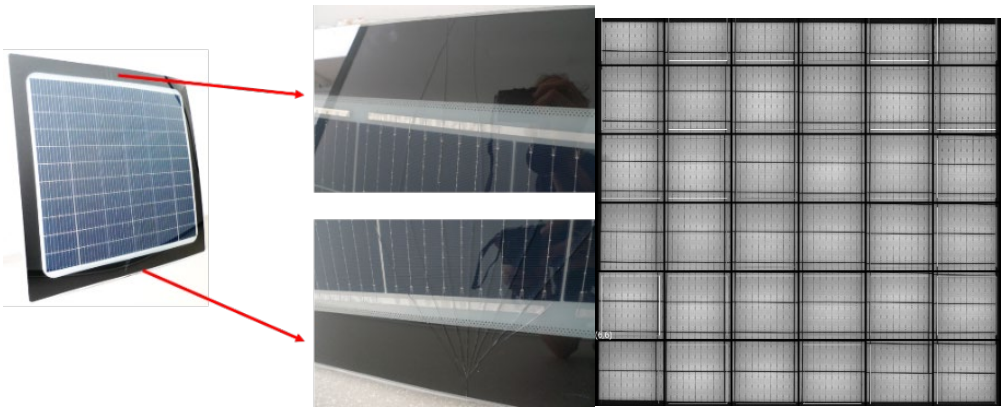

Figure 18: Despite the crack in the front glass (left), the solar cells inside are not affected (right) (curved glass courtesy of AGP eGlass)

Table 6: Performance of 2 PV sunroofs indicating the increase (in short circuit current Isc) due to the use of a more transparent front glass (measurement error < 2%)

	I_{sc} [A]	V_{oc} [V]	FF [%]	P_{mpp} [W]
Trial 1	4.344	45.048 (66x 0.683)	81.7	159.8 (66x 2.421)
Trial 2	4.717	45.070 (66x 0.683)	81.5	173.2 (66x 2.625)
increase	+8.6%	+0.0%	-0.2%	+8.4%

Additionally, we also prepared another sunroof using our multi-wire interconnection technology from the Section 2. The result, including performance and EL picture, is shown in Figure 19. The optical pictures also illustrate the aesthetics in comparison to the implementation with standard half-cell PERC strings. For both laminates, the same lamination recipe was used.

Figure 19: Optical comparison between sunroof with standard 9BB half-cell PERC strings (left) and 6x6 MW interconnected cells (centre), with EL picture and IV performance of the latter (right) (curved glass courtesy of AGP eGlass)

3.3 (VIPV) application 2: light-weight bonnet

Apart from the sunroof's PV integration, where anyway glass-glass was required as a boundary condition, many VIPV applications require minimal weight. In other publications [23-25] we have elaborated our approach towards fibre reinforced encapsulants (GFRE) and back covers (GFRB), including results on reliability testing as TC, DH and HF as well as UV exposure and hail impact testing. Figure 20 indicates the minimal additional weight of integrating PV on top of the existing metal (steel) pieces. In this work, we implement our GFRB approach next to a direct integration on the steel surface of a car bonnet, shown in Figure 21. In this case, shingling technology [5] was applied in an effort to maximize the active (Si cell) area on this complex and curved surface. The full bonnet measures roughly 1.00 x 1.40 m^2 (outer dimensions). In first instance we tested cutout pieces of the bonnet for the lamination.

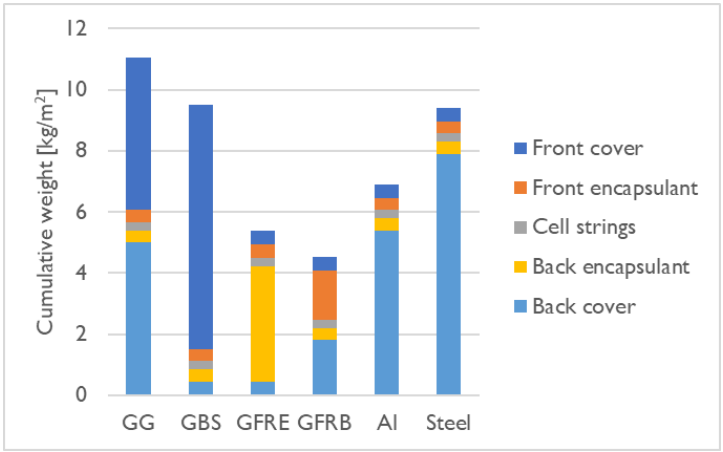

Figure 20: Typical weight distribution of various module buildups: glass-glass (GG), glass-backsheet (GBS), glass fibre reinforced encapsulant (GFRE), glass fibre reinforced back cover (GFRB), and implementation on 2 mm thick aluminum (Al) and 1 mm thick steel (steel) back covers

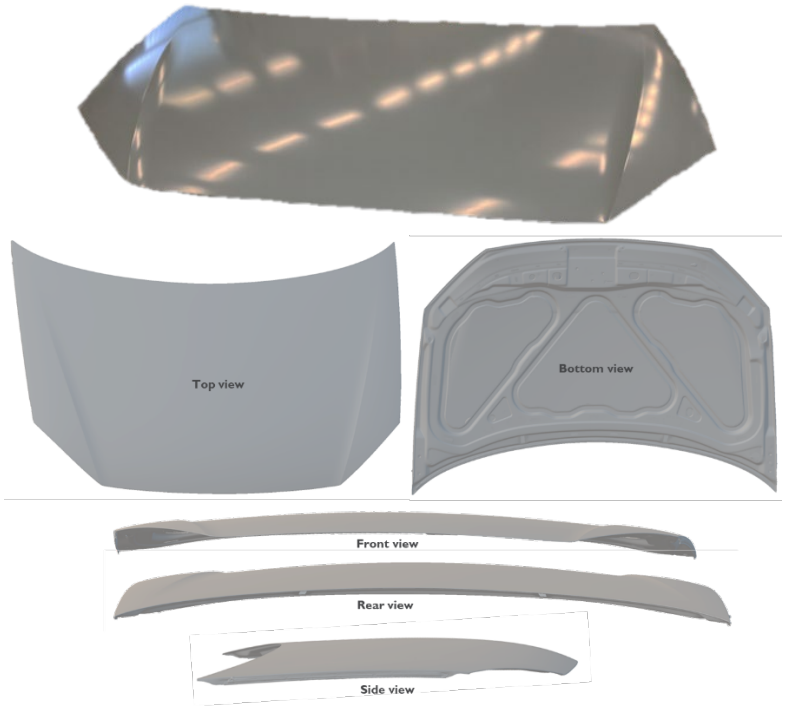

Figure 21: Picture (top) and 3D scan impressions (bottom) of the car bonnet used for PV integration trials

Figure 22 shows a steel car bonnet part embedding a string of 9 BB 6 half PERC cells before and after lamination, and the resulting performance is reported in Table 7. For aesthetical reasons, we included a black backsheet and a transparent frontsheet. In this case, for integrating PV on the bonnet (piece), the weight increases from 2.56 to 3.16 kg.

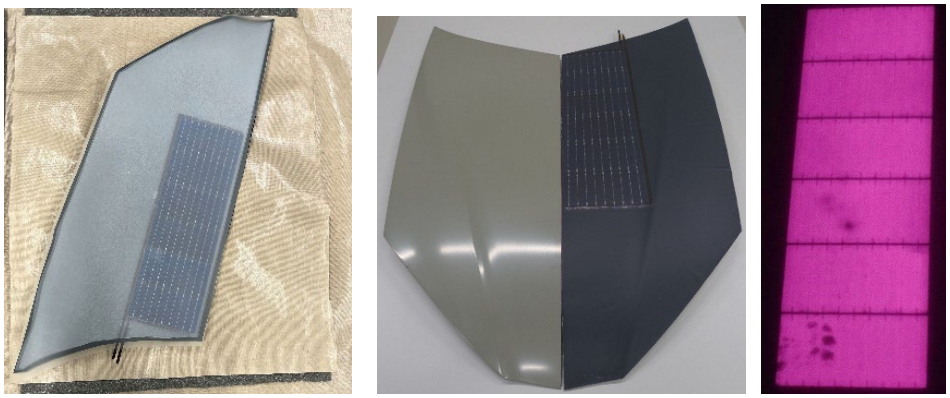

Figure 22: PV on an steel bonnet piece: layup (left), comparison before/after (middle) and resulting EL (right)

Table 7: Performance parameters of PV on the steel bonnet piece from Figure 22

I_{sc} [A]	V_{oc} [V]	FF [%]	P_{mpp} [W]
4.69	4.17	80.9	15.8

Similarly, we also fabricated a version where we replaced the steel back cover with a GFRB back cover. First, we "duplicated" the bonnet piece using the steel part as a mould in a separate double-membrane lamination. For this, the temperature needs to be sufficiently high to melt the polymer matrix of the GFRB material. In this case, the polymer matrix of the GFRB consists of polypropylene (PP) material, which we melt at 175-180°C. Afterwards, we used a

string of shingled SHJ cells to fabricate the PV laminate at a lower lamination temperature (below the melting temperature of the GFRB polymer). This is illustrated in Figure 23, and the resulting performance is given in Table 8. In this case, the weight is reduced from 2.56 to 1.06 kg (although a support structure still needs to be added for a fair comparison).

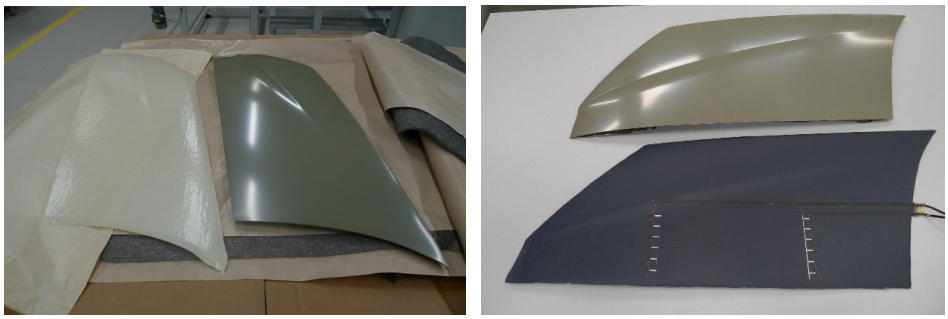

Figure 23: PV on a GFRB bonnet piece: GFRB duplication of the bonnet piece (left), comparison before/after (right)

Table 8: Performance parameters of PV on the GFRB bonnet piece from Figure 23

I_{sc} [A]	V_{oc} [V]	FF [%]	P_{mpp} [W]
1.25	8.84	79.3	8.8

Finally, trials have been made to upscale this last approach. The first attempt is illustrated in Figure 24 and Table 9. While the EL picture before lamination shows that the 4 strings (with shingled cell interconnection) are clearly curved along the bonnet, after lamination the frontsheet is severely wrinkled, and the underlying cells are significantly cracked in those areas.

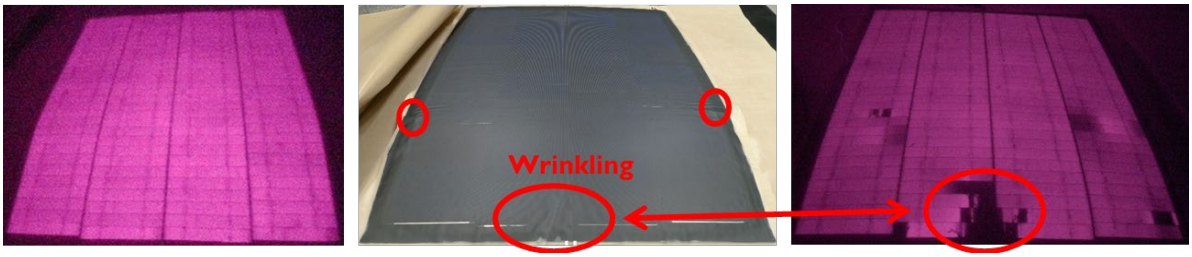

Figure 24: Severe wrinkling of the stiff back-and frontsheets induces cell cracks after lamination (central optical picture and right EL picture) in the shingled strings have no cracks whatsoever prior to lamination (left EL picture)

Table 9: Performance parameters of shingled PV on GFRB from Figure 24

I_{sc} [A]	V_{oc} [V]	FF [%]	P_{mpp} [W]
4.924	21.992	75.3	82

In our current hypothesis, this wrinkling may be due to the non-melting stiff back- resp. frontsheet that cover the full surface behind resp. in front of the cells that cannot conform to the complex (multi-dimensional) curvature of the bonnet. That would mean, to avoid this wrinkling, it is necessary to either cut up these sheets such that they do not experience as much this complex curvature, or adapt this material to enable it to plastically deform during lamination.

With this in mind, another bonnet was fabricated for the test, where the black backsheet was limited to stripes, and only implemented in the areas in between the shingled strings and at the edge of the module. An alternative solution here could be to provide colouring in the bulk of the GFRB, or painting/coating it prior to layup. The frontsheet was not applied, instead a very thin

release foil prevented the frontside encapsulant from being exposed during lamination. The results shown in Figure 25 and Table 10 indicate that this indeed avoids the significant wrinkling and associated cracking. However, many small wrinkles are observed across the full surface, which is probably due to the very thin release foil that is likewise not plastically deforming. Rather it deforms out-of-plane during lamination to deal with the excess material when it is pressed against the complex curved surface. This out-of-plane deformation then results in an imprint into the molten encapsulant layer.

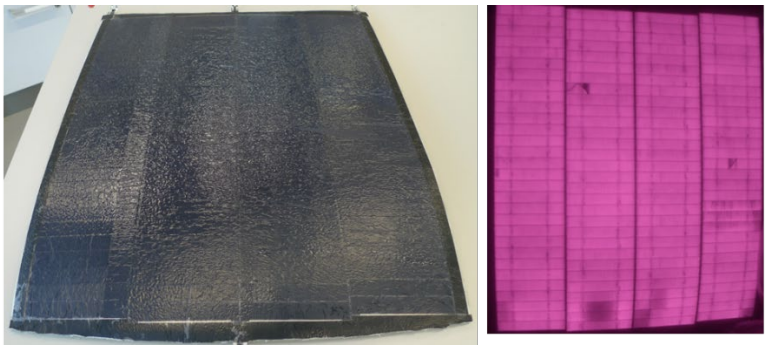

Figure 25: Optical (left) and EL picture (right)indicating the absence of severe wrinkling and cracking by leaving out the full-area backsheet and frontsheet

Table 10: Performance parameters of shingled PV on GFRB from Figure 25

I_{sc} [A]	V_{oc} [V]	FF [%]	P_{mpp} [W]
5.687	22.090	78.3	98

Upscaling further, we prepared a full-size bonnet with a similar GFRB buildup, with the results shown in Figure 26 and Table 11. Additional to the bonnet surface itself, we also implemented the steel supporting structure to provide a mechanical demonstrator and to indicate the weight differences. The basic bonnet weighs 10.4 kg, of which 3.9 kg is taken up by the supporting structure, while the top surface is 6.5 kg. The light-weight GFPP laminate as top surface replacement weighs 4.1 kg, so the total full-size bonnet weighs 8.0 kg. This means it is 2.4 kg lighter than the basic bonnet at 10.4 kg. Of course testing is still required to determine the impact of replacing the steel top surface in its (thermo-)mechanical behaviour.

Figure 25: Fabricated full-size bonnet with a GFRB-based top surface and the original steel supporting structure: optical pictures of front (top left) and rear (top centre) and EL picture (top right), as well as a picture of the implementation on a car (bottom)

Table 10: Performance parameters of shingled PV on full-size GFRB bonnet from Figure 25

I_{sc} [A]	V_{oc} [V]	FF [%]	P_{mpp} [W]
6.21	22.143	80.6	111

As work in progress on the fabrication technology, next steps are to look into either plastically deforming the frontsheet material, or using preformed frontsheets, potentially combined with stretchable materials that can act as release layer. Of course, other possibilities can be conceived, e.g. based on liquid encapsulation, or coating techniques such as painting, but this is beyond the scope of the work reported here.

4. SUMMARY

In this paper we report on the technologies we are developing to address the growing market for integrated PV applications. In particular, the underlying targets are to improve aesthetics, with maximal performance, to accommodate PV also on curved surfaces, and to reduce weight, each separately or combined opening up more applications and potential PV deployment. We mix examples targeting building and automotive applications, to illustrate the variety of requirements (colours, curvature, weight, reliability, safety), although this variety within building and vehicle applications is probably as large as between them.

In terms of interconnection, we share the evaluation of our multi-wire interconnection, in terms of performance and reliability. While the potential is promising, and the technology can pass some basic IEC testing in terms of thermal cycling, damp heat and humidity freeze, some further improvement is desirable. This includes also increasing statistics and comprehensive and reproducible testing to determine a "technology" window in terms of materials and process conditions.

To illustrate the application of this interconnection technology, we subsequently demonstrate it in BIPV laminates, indicating the aesthetics with a front glass that may be coloured, as well as

for semi-transparent applications where the distance between cells can be increased. In both cases, the versatility of the technology allows a customizable layout with minimized bussing requirements.

Further on, towards curved surfaces, we demonstrate the successful integration of PV (including the multi-wire interconnection) into a curved glass-glass sunroof. This is achieved using a PV (membrane) lamination technology, albeit in a somewhat modified (double-membrane) configuration to allow for the curvature.

Finally, we elaborate our progress on our technology development towards light-weight applications. Here we demonstrate our GFRB strategy for a car bonnet, using the same lamination technology for curved surfaces as for the sunroof, but this time using the original bonnet as a mould to make the glass fibre reinforced back cover as well as the final laminate. We indicate the achieved performance in terms of IV, EL and weight, and discuss some remaining issues to be addressed next, in particular the wrinkling and its associated risk on cracking in case of a multi-dimensionally curved surface, as well as the (thermo)mechanical impact of implementing such light-weight alternatives.

ACKNOWLEDGMENT

The authors gratefully acknowledge the Flemish government for its financial support through the funded ICON projects SNROOF, DAPPER and CSP+ and the involved project partners, as well as the European Union's Horizon 2020 Programme for research, technological development and demonstration for funding part of this work under Grant Agreement no. 857793 (HighLite). In particular, we want to thank CEA-INES and Applied Materials Baccini for supplying strings of shingled SHJ cells and FlandersMake for the implementation of the bonnet on a car. The authors also would like to acknowledge the partial funding by the Kuwait Foundation for the advancement of Sciences under project number P115-15EE-01.

REFERENCES

[1] IEA-PVPS Task 17. "State-of-the-Art and Expected Benefits of PV-Powered Vehicles". report T17-01 (2021)
[2] Picture from https://forum.solar-electric.com/discussion/349939/can-anybody-identify-this-really-old-module
[3] Picture from https://www.clean-energy-ideas.com/solar/solar-panels/monocrystalline-vs-polycrystalline-solar-panels/
[4] Picture from https://www.trinasolar.com/us/product
[5] D. Tonini, G. Cellere, M. Bertazzo, A. Fecchio, L. Cerasti, M. Galiazzo. "Shingling Technology For Cell Interconnection: Technological Aspects And Process Integration". Energy Procedia. 150. 36-43, doi: 10.1016/j.egypro.2018.09.010 (2018).
[6] E. Van Kerschaver, G. Beaucarne. "Back-contact solar cells: a review". Progress in Photovoltaics: Research and Applications 2006, Vol. 14, pp. 107–123. DOI:10.1002/pip.65714 (2006)
[7] https://www.agc-yourglass.com/en-BE/brands/artlite-digital
[8] C. Ballif, L.E. Perret-Aebi, S. Lufkin, E. Rey. "Integrated thinking for photovoltaics in buildings". Nature Energy 2018, Vol. 3, pp. 438–442. https://doi.org/10.1038/s41560-018-0176-2 (2018)
[9] J. van Roosmalen, L. Slooff, L. Okel, M. van den Donker, T. de Vries, T. Minderhoud, N. Wang, G. Gijzen, T. Sepers, M. Rietbergen, L. Polinder, R. Heller, A. Versluis, F. Frumau. "Brick modules for improved aesthetics in PV, Introducing the Dutch Solar Design project". Advanced Building Skins Conference, Bern Switzerland (2017)

[10] T. Gewohn, M. R. Vogt, B. Lim, C. Schinke, R. Brendel. "Postproduction Coloring of Photovoltaic Modules With Imprinted Textiles". IEEE Journal of Photovoltaics, Vol. 11, no. 1, pp. 138-143, doi: 10.1109/JPHOTOV.2020.3034001 (2021)
[11] A. Morlier, B. Lim, S. Blankemeyer, H. Schulte-Huxel, R. Witteck, T. Daschinger, S. Bräunig, M. Köntges, R. Brendel. "Photovoltaic Modules with the Look and Feel of a Stone Façade for Building Integration". Solar RRL. DOI:10.1002/solr.202100356 (2021)
[12] PVPS Task 15 "Coloured BIPV: Market, Research and Development". Report T15-07 (2019)
[13] B. Bläsi, T. Kroyer, T.E. Kuhn. O. Höhn. "The MorphoColor Concept for Colored Photovoltaic Modules". IEEE Journal of Photovoltaics, vol. 11, no. 5, pp. 1305-1311, Sept. 2021, doi: 10.1109/JPHOTOV.2021.3090158.
[14] Mitrex. Intersolar exhibition 2022, buildup specified in https://www.mitrex.com/solar-facade/
[15] G. Cattaneo, A. Faes, H.Y. Li, F. Galliano, M. Gragert, Y. Yao, R. Grischke, T. Söderström, M. Despeisse, C. Ballif, L.E. Perret-Aebi. "Lamination process and encapsulation materials for glass–glass PV module design". Photovoltaics International Vol. 82 (2015)
[16] L. Galuppi, G. Royer-Carfagni. "Optimal cold bending of laminated glass". International Journal of Solids and Structures, Vol. 67–68, pp. 231-243, https://doi.org/10.1016/j.ijsolstr.2015.04.023 (2015)
[17] D. Sato, N. Yamada. "What are the Differences between VIPV and conventional PV? ~ Prototyping a 3D curved PV module". 4th PVTEC webinar (2021)
[18] https://www.pv-magazine.com/spotlights/no-limitations-in-lamination/
[19] A.C. Martins. "Glass-free lightweight PV building elements: solutions to minimize weight and maximize durability". PhD thesis (2019)
[20] N. Yurrita, J. Aizpurua, W. Cambarau, G. Imbuluzqueta, J.M. Hernández, F.J. Cano, I. Huerta, E. Rico, T. del Caño, S. Wölper, F. Haacke, O. Zubillaga. "Composite material incorporating protective coatings for photovoltaic cell encapsulation". Solar Energy Materials and Solar Cells, Vol. 245, 111879, https://doi.org/10.1016/j.solmat.2022.111879 (2022)
[21] J. Govaerts, T. Borgers, R. Van Dyck, N. Andries, P. Meyers, A. van der Heide, J. Poortmans. "Encapsulant-Integrated Interconnection of Bifacial Solar Cells for BIPV Applications: Latest Results in the Twill-BIPV Project". EUPVSEC 2020, p. 33-37 (2020)
[22] T. Borgers, J. Govaerts, "Methods for electrically contacting and interconnecting photovoltaic cells". Patent application submitted (EP 3 790 059 A1) (2019)
[23] B. Luo, J. Govaerts, R. Van Dyck, M. Casasola Paesa, T. Borgers, A. van der Heide, F. Lisco, M. Daenen, A. Willem Van Vuure, J. Poortmans, "Reliability Assessment and Development of Ultra-Lightweight PV Modules Towards Vehicle-Integrated Photovoltaics". WCPEC-8 (2022)
[24] B. Luo, J. Govaerts, R. Van Dyck, T. Borgers, B. Ruttens, M. Casasola Paesa, J. D'Haen, L. Tous, H. S. Radhakrishnan, M. Daenen, A. W. van Vuure, J. Poortmans. "Development and Thermo-mechanical Reliability Assessment of Fiber Reinforced Polymers in Lightweight PV Modules towards Vehicle-integrated Photovoltaics". (submitted to SolMat)
[25] J. Govaerts, B. Luo, T. Borgers, R. Van Dyck, A. van der Heide, L. Tous, A. Morlier, F. Lisco, L. Cerasti, M. Galiazzo, J. Poortmans "Development and testing of light-weight PV modules based on glass-fibre reinforcement". EPJ Photovoltaics Vol. 13 DOI: 10.1051/epjpv/2022007 (2022)